Spectral Characterization of Agricultural Burned Areas for Satellite Mapping

A Thesis
Presented in Partial Fulfillment of the Requirements for the
Degree of Master of Science
with a
Major in Natural Resources
in the
College of Graduate Studies
University of Idaho
by

Erik J. Boren

Major Professor: Luigi Boschetti, Ph.D.
Committee Members: Alistair Smith, Ph.D.; Jessica McCarty, Ph.D.; Pietro Ceccato, Ph.D.
Department Administrator: Anthony Davis, Ph.D.

May 2015

Authorization to Submit Thesis

This thesis of Erik J. Boren, submitted for the degree of Master of Science with a Major in Natural Resources and titled "Spectral Characterization of Agricultural Burned Areas for Satellite Mapping," has been reviewed in final form. Permission, as indicated by the signatures and dates below, is now granted to submit final copies to the College of Graduate Studies for approval.

Major Professor: _____ Date:_____
Luigi Boschetti, Ph.D.

Committee Members: _____ Date:_____
Alistair Smith, Ph.D.

_____ Date:_____
Jessica McCarty, Ph.D.

_____ Date:_____
Pietro Ceccato, Ph.D.

Department Administrator: _____ Date:_____
Anthony Davis, Ph.D.

Abstract

Burned area detection with remotely sensed satellite data in agricultural landscapes is not only necessary for the estimation of global biomass burning emissions, but also has gained attention from managers interested in improved methods for the quantification of local scale emissions which affect air quality and human health. Mapping agricultural burned areas accurately, precisely and reliably, with methods that can be applied globally, is difficult because of the spectral and temporal characteristics of agricultural regions and prescribed cropland fires. These challenges have not been fully addressed by the scientific literature. Chapter 1 of this thesis presents an extensive literature review on the methods currently used for agricultural burned area mapping. Chapter 2 presents original research on the spectral characterization of agricultural burned areas, using field data and mixture models to analyze the response of spectral indices to the changes induced by fire and agricultural practices. The conclusions summarize the significance of the presented research for understanding the potential and limits of satellite data for agricultural burned area monitoring, and outline the directions for future work.

Acknowledgements

I would like to first thank everyone on my committee, Dr. Alistair Smith, Dr. Jessica McCarty and Dr. Pietro Ceccato for their support as well as my advisor: Dr. Luigi Boschetti for all the mentoring he provided. I would like to extend my special thanks to Dr. Donald Zak at the University of Michigan and Dr. Jessica McCarty at the Michigan Technological Research Institute. Both mentors have been great scientific role models and have had significant influences on the path I have chosen to pursue academically and professionally. This degree would not be possible if it were not for the funding provided by the National Aeronautics and Space Administration (NASA) and United States Department of Agriculture (USDA).

Dedication

I would like to dedicate this work to my high school chemistry teacher who will be retiring after the 2014-2015 academic year: Mrs. Cheryl Wells. Thank you for all you've done and for the young scientists you've inspired throughout 40 years of teaching.

Table of Contents

List of Figures

List of Tables

Chapter 1: Mapping Burned Cropland Area from an Integration of MODIS Products: a Literature Review

Abstract

Burning of agricultural residue is a widespread practice, resulting in the emission of gases and particulate matter in the atmosphere: interest in accurately and reliably quantifying agricultural burned area is rising, due to implications for atmospheric chemistry and air quality. Satellite data is a potential solution for detecting the occurrence of cropland fires. In particular, data from the Moderate Resolution Imaging Spectrometer (MODIS) have been widely used for cropland fire monitoring. The present chapter reviews the current state of research and literature and summarizes the methodologies that have been adopted. Presently, two primary methods are used to estimate crop fire occurrence with MODIS data: the use of active fire detections from the MOD14/MYD14 global active fire product integrated over time, and the direct detection of burned areas using changes in the Normalized Burn Ratio (NBR) spectral indices in conjunction with active fire detections. As it not realistic to quantify agricultural burning with ground survey methods, satellite data monitoring is the only practical solution, especially at continental and global scale. In light of the inherent uncertainties in the available methodologies, the accuracy of the satellite-based agricultural burned area detections is not fully quantified.

Introduction

Agricultural burning has significant impact on carbon emissions, air quality, and human health (Korontzi *et al.* 2006; McCarty *et al.* 2008; McCarty 2011; Melvin 2012). Timely and accurate quantification of the temporal and spatial variability of the fires is

needed, not only to improve emission inventories, but also for decision support for the development of informed legislative measures to mitigate air pollution from agricultural residue burning (Aneja *et al.* 2006). National statistics of agricultural burning are derived from surveys and self-reporting by producers, and are often incomplete and inhomogeneous (Dennis *et al.* 2002), making remote sensing the only realistic approach for systematic monitoring at the national, continental or global scale (Feng and Christopher 2013).

This review presents the current state of the art coarse resolution (500-m to 1-km) mapping of cropland fires with the Moderate Resolution Imaging Spectroradiometer (MODIS) instrument. We found a total of nine published studies, presenting a variety of methods and results for detecting agricultural fires. Several factors that contribute to variations and uncertainties in results are identified.

For the purpose of this review, the terms agricultural and cropland fires are used interchangeably, and are defined as the management practice of using prescribed fires to remove crop residues, senescent vegetation, and undesirable natural vegetation (e.g. weeds or shrubby encroachment). Understanding landscape management techniques and the implications for our environment as well as a remote sensing techniques being used to analyze agricultural burning is essential.

Agricultural Fire Emissions

Many producers use burning as a tool for managing croplands (Dennis *et al.* 2002;Korontzi *et al.* 2006; McCarty *et al.* 2007). Depending on the crop type and management technique, prescribed agricultural field burning can occur during the harvesting, post-harvesting or pre-planting periods (Huang *et al.* 2012). The practice is used as an inexpensive means for increasing fertilization effectiveness, eliminating pests and weeds, and

thinning excess crop residue for enhancing seeding productivity (Canode and Law 1979; Lamb and Murray 1999).The most cultivated crops globally are the cereal crops of wheat, maize, rice, barley, millet and sorghum which occupy more than two thirds of agricultural land area (Leff *et al.* 2004). The cereal crop residues along with the residues of sugar cane, soy, and cotton provide most of the agricultural biomass burned (Yevich and Logan 2003). Compared to fires of forest and grassland fires, the low fuel load in agricultural burning results in typically shorter duration and lower emitted energy (Sharma *et al.* 2009).

Emissions from these fires contribute to atmospheric trace gases and particulate matter that alter atmospheric chemistry and may contribute to global climate change (Crutzen and Andreae 1990; Dennis *et al.* 2002), including short-lived climate forcers like black carbon (McCarty *et al.* 2012; Bond *et al.* 2013). Greenhouse gases released from crop residue burning include carbon dioxide, carbon monoxide, methane, non-methane-hydrocarbons, nitric oxide, nitrous oxide, and atmospheric particulate matter (Crutzen and Andreae 1990). According to the analysis by Korontzi *et al.* (2006), agricultural areas account for approximately 8-11% of all global active fire detections, and are the fourth most common land cover class for fire activity. Because croplands are often in proximity of densely populated areas, despite the relatively low amount of burned biomass, agricultural fires have a significant impact on air quality and human health (McCarty 2011).

Agricultural land constitutes more than 10% of the global land surface and is likely to expand as a result of growing demands for food and agricultural products caused by increasing human populations (Smith *et al.* 2010). Having the ability to characterize crop residue burning with accuracy and reliability is an existing challenge for scientists and managers interested in monitoring air quality emissions. In addition, spatially explicit, near

real time detection of agricultural fires is essential to monitor compliance, and for enforcing local regulations on prescribed fires.

Overview of the MODIS instruments

The MODIS instrument, aboard the polar orbiting EOS-AM1 (Terra) and EOS-PM1 (Aqua) satellites of the National Aeronautics and Space Administration (NASA) Earth Observing System (EOS), was the first sensor designed with spectral bands specifically designed for fire detection (Kaufman *et al.* 1998). The two satellites are placed on a low altitude, sun-synchronous polar orbit, which they cover in descending (Terra) and ascending nodes (Aqua). The wide swath of MODIS ensures that at least one instrument overpasses during the day and one at night for the whole globe and more than two at latitudes greater than 40^{o} (Wolfe *et al*. 1998). The high temporal resolution, along with instrument's spectral detection capabilities, makes MODIS a preferred instrument for scientists interested in fire detection. Besides the fire products, an extensive suite of systematic thematic products for environmental monitoring has been systematically produced for the entire duration of the MODIS mission (2000 onwards), including spectral albedo, vegetation indices, land cover, snow and ice cover, and a number of biophysical variables for the computation of hydrological balances, biogeochemistry, and global carbon cycles (Justice *et al*. 1998; Running *et al.* 1994). Table 1 lists all MODIS bands with associated spatial scale and primary scientific purpose.

Table 1. Channel specifications for the MODIS sensor (modified from McCarty *et al.* 2008)

Band	Bandwidth (μm)	Spatial Resolution (m)	Primary Scientific Purpose
1	0.620 - 0.670	250	Vegetation chlorophyll absorption Land cover transformations Cloud / edge detection / masks
2	0.841 - 0.876	250	Cloud / vegetation / water / edge detection Land-cover transformations / masks
3	0.459 - 0.479	500	Soil and vegetation differences
4	0.545 - 0.565	500	Green vegetation
5	1.230 - 1.250	500	Leaf and canopy properties
6	1.628 - 1.652	500	Snow and cloud differences / masks
7	2.105 - 2.155	500	Land and cloud properties
8	0.405 - 0.420	1000	Water color (chlorophyll / pigments / sediments) Atmospheric scattering / cloud masks
9	0.438 - 0.448	1000	Water color
10	0.483 - 0.493	1000	Water color
11	0.526 - 0.536	1000	Water color
12	0.546 - 0.556	1000	Sediments
13	0.662 - 0.672	1000	Sediments, atmosphere
14	0.673 - 0.683	1000	Chlorophyll fluorescence
15	0.743 - 0.753	1000	Aerosol properties
16	0.862 - 0.877	1000	Aerosol and atmospheric properties
17	0.890 - 0.920	1000	Water vapor / atmospheric properties
18	0.931 - 0.941	1000	Water vapor / atmospheric properties
19	0.915 - 0.965	1000	Water vapor / atmospheric properties
20	3.660 - 3.840	1000	Sea surface temperature
21	3.929 - 3.989	1000	Forest fires / volcanoes
22	3.929 - 3.989	1000	Cloud
23	4.020 - 4.080	1000	Cloud / surface temperature / cloud mask
24	4.433 - 4.498	1000	Cloud / surface temperature / cloud mask
25	4.482 - 4.549	1000	Tropical temperature / cloud fraction
26	1.360 - 1.390	1000	Cirrus cloud / cloud mask
27	6.535 - 6.895	1000	Tropical temperature / cloud fraction
28	7.175 - 7.475	1000	Mid-tropical humidity
29	8.400 - 8.700	1000	Upper-tropical humidity
30	9.580 - 9.880	1000	Total ozone
31	10.780 - 11.280	1000	Cloud / surface temperature
32	11.770 - 12.270	1000	Cloud / surface temperature
33	13.185 - 13.485	1000	Cloud height and fraction
34	13.485 - 13.785	1000	Cloud height and fraction
35	13.785 - 14.085	1000	Cloud height and fraction
36	14.085 - 14.385	1000	Cloud height and fraction

Only two bands (red and near infrared [NIR]) have a spatial resolution of 250-m and allow for the computation of the normalized difference vegetation index (Huete et al, 1999). The 500-m bands cover most of the wavelengths commonly used for terrestrial monitoring with optical remote sensing data, with the exception of the thermal bands, which are available at 1000-m.

The MODIS products are subject to systematic quality assessment and to periodic reprocessing of the whole data record. Reprocessing improves the quality of the MODIS products, by using the latest calibration information, and by using improved algorithms. Once reprocessed, the updated inventory of MODIS data is referred to as a collection (Giglio 2010). The collections advance from collection 1, Terra's first set of data, to the current set, collection 5.

MODIS Fire Products

Two fire products are part of the MODIS land suite: an active fire product and a burned area product (Justice *et al.* 2002). The global active fire product (MOD14/MYD14) maps fires that are actively burning at the time of the satellite overpass, detected as thermal anomalies at 1-km pixel resolution (Giglio *et al.* 2003). The second product is the MODIS global burned area product (MCD45A1) which detects the changes induced by fire on the vegetation, using a bi-directional reflectance model at 500-m^2 resolution (Roy *et al.* 2002; Roy *et al.* 2005). The MODIS fire products are distributed from the Earth Resources Observation Systems Data Center (EDC) Distributed Active Archive Center (DAAC) (Justice *et al.* 2002). Currently, active fire data sets are available through the Fire Information for Resource Management System (FIRMS) which is publically accessible on-line (Davies *et al.*

2009). Additionally, GIS- ready (geotiff, shapefile) versions of the MODIS burned area products are distributed by the University of Maryland (http://modis-fire.umd.edu/).

The MODIS active fire detection algorithm (Giglio *et al*. 2003) was developed based on heritage algorithms developed for the Tropical Rainfall Measuring Mission (TRMM) Visible and Infrared Scanner (VIRS) and Advanced Very High Resolution Radiometer (AVHRR) systems (Kaufman *et al.* 1990; Giglio *et al.* 1999). The algorithm uses a contextual approach, flagging a pixel as a thermal anomaly if its temperature is either (1) higher than a very strict set of absolute thresholds or (2) higher than a less strict set of thresholds, but also significantly higher than the surrounding pixels. The algorithm uses brightness temperatures derived from MODIS bands 21 and 22, (3.6-4.0 μm) and 31 (10.8-11.2 μm).

The active fire detection takes advantage of the high saturation temperature of the MODIS bands: Band 21 saturates at nearly 500 K (while band 22 saturates at 331 K and is used instead of band 21 at low temperature) and Band 31 saturates at approximately 400 K. Other channels are used in the detection algorithm for correction purposes, like masking, false alarm rejection, sun glint, etc., are presented in table 2.

Table 2. MODIS channels used in detection algorithm (modified from Giglio *et al.* 2003)

Band	Central wavelength (μm)	Purpose
1	0.65	Sun glint and coastal false alarm rejection; cloud masking
2	0.86	Bright surface, sun glint, and coastal falst alarm rejection; cloud masking
7	2.1	Sun glint and coastal false alarm rejection
21	4	High-range channel for active fire detection
22	4	Low-range channel for active fire detection
31	11	Active fire detection, cloud masking
32	12	Cloud masking

The active fire detection product has undergone successive modification in response to persistent problems including false alarms in sparsely vegetated areas and an inability to detect small fires (Justice *et al.* 2002; Giglio *et al.* 2003). Nevertheless, weaknesses of the

algorithm have been demonstrated. Detection rates have been shown to decrease for fires underneath heavy cloud cover or smoke (Csiszar *et al.* 2006; Hawbaker *et al.* 2008). Overpass timing is also an inherent limitation, as the instrument only detects fires that are actively burning at the time of overpass. The diurnal cycle of fire activity makes it more likely to detect burns in the afternoon, when weather conditions are most favorable, so combining products from both satellites is important as Terra and Aqua daytime overpasses are at 10:30 am and 01:30 pm respectively, and the nighttime overpasses at 10.30 pm and 1.30 am (Hawbaker *et al.* 2008; Korontzi *et al.* 2008; Giglio 2010). Because of the fundamental laws of radiation, emitted power is a function of the fourth power of the temperature of a surface. As a consequence, the thermal emission detected from a pixel containing an active fire is orders of magnitude greater than a pixel with no fire, allowing for the reliable detection of subpixel fires, much smaller than 1-km^2 (Giglio *et al.* 2006; Huang *et al.* 2012). However, the detection rate still has a direct relationship with fire size, showing that detection rate decreases as the fire size decreases (Hawbaker *et al.* 2008).

The MODIS burned area product provides temporal and spatial information on burned areas that the active fire detection algorithm, because of its binary nature, is unable to do on its own (Roy *et al.* 2005). The burned area product is derived from a bi-directional reflectance model-based change detection algorithm which is applied independently to geolocated pixels over a time series (weeks to months) of reflectance data (Roy *et al.* 2002). Due to the small size and quick transition of burned agricultural fields to plowed fields and because the burned area product was developed for detecting burned area in grassland and wildland landscapes, the algorithm underestimates systematically the extent of agricultural fires, and is not a suitable source of data for agricultural fire monitoring (J.L. McCarty, Michigan Tech

Research Institute, personal communication). The MCD45A1 burned area product has been applied in past literature as a means to quantify burned cropland area due to the lack of existing regional products (Chang and Song 2010; Song *et al.* 2010), but has severe limitations. Most of the current literature, instead, relies on two main methods for mapping cropland fire; a combination of MOD14/MYD14 active fire products with land cover data sets to derive spatial and temporal information about fire occurrence, and a hybrid remote sensing methodology which combines 8-day difference normalized burn ratio (dNBR) composite area with MOD14/MYD14 active fire detections.

Mapping Agricultural Fires with MODIS data: State of the Art

A review of the literature revealed that all nine studies used the active fire products either produced from MODIS Terra or both MODIS Terra and Aqua instruments, MOD14 and MYD14 respectively (Table 3). All the studies used a land cover product (most often a MODIS derived land cover product) to determine the spatial and temporal distribution of fires in different land cover classes.

The earliest works combined active fire products with land cover data sets to isolate agricultural fires, to then study spatial and temporal patterns of cropland fire distribution. Korontzi *et al.* (2006) acquire and combined MODIS Terra active fire detections (MOD14) globally, for the 2001-2003 period. Only MODIS-Terra detections were considered, due to the unavailability of Aqua MODIS data until the launch in April 2002. The MODIS MOD12 land cover product (Friedl *et al.* 2002) was used to stratify the active fire detections by landcover, and extract the agricultural fires. The MOD12 land cover data set was created using a database of global exemplary land cover points as inputs to a supervised classifier algorithm (Loveland and Belward 1997). The cropland fire activity was analyzed in terms of inter-

annual variability of fire occurrence and spatial distribution of fire event at the global and regional scale.

This was the first comprehensive study of agricultural fire activity: it outlined for the first time the global spatial and temporal patterns of cropland occurrence. The study raises important questions about what significant factors are controlling spatial and temporal variables of cropland fire events, and it calls for the need of research for examining the spatial and temporal relationships as well as the ability for assessing cropland burned area. The methods used in this study are used in the majority of subsequent studies examining cropland fire occurrences on regional scales (Table 3).

As noted, none of the selected studies made use of the MCD45A1 burned area product due to the unsuitable characteristics of the algorithm for mapping agricultural field burning or were conducted before the MCD45A1 product was made widely available to the scientific community. Instead, attempts have been made to develop a dedicated methodology for mapping burned cropland areas. Of the nine studies, three used the MODIS reflectance product (MOD09A1) to compute the dNBR spectral index, to then proceed to map burned areas. The dNBR index is derived from the differencing of pre-fire and post-fire MODIS surface reflectance NBR products (NBR= $Band_2$-$Band_7$/$Band_2$+$Band_7$). McCarty *et al.* (2008) were the first to present and demonstrate the use of this hybrid methodology.

The hybrid approach is summarized in a conceptual model (Fig. 1). The total burned cropland area is the sum of calibrated active fire counts and dNBR burned area detections. The MODIS active fire product is calibrated to assign detections the average corresponding burned area. Mc Carty et al (2008) proposes a value of 0.16-km^2 which is 16 ha or ~40 acres for this calibration. The dNBR was calculated as the difference between the pre-burn NBR

values and NBR values of an image taken 8 days later. A region specific threshold was calculated in order to exclude unrelated spectral changes, for example derived from tillage. The threshold was created by identifying burned fields on the ground in two field campaigns, and by observing the changes in NBR over these known prescribed agricultural burned areas. The results from validating the hybrid burned area product with field data and high-resolution imagery are summarized in Table 3.

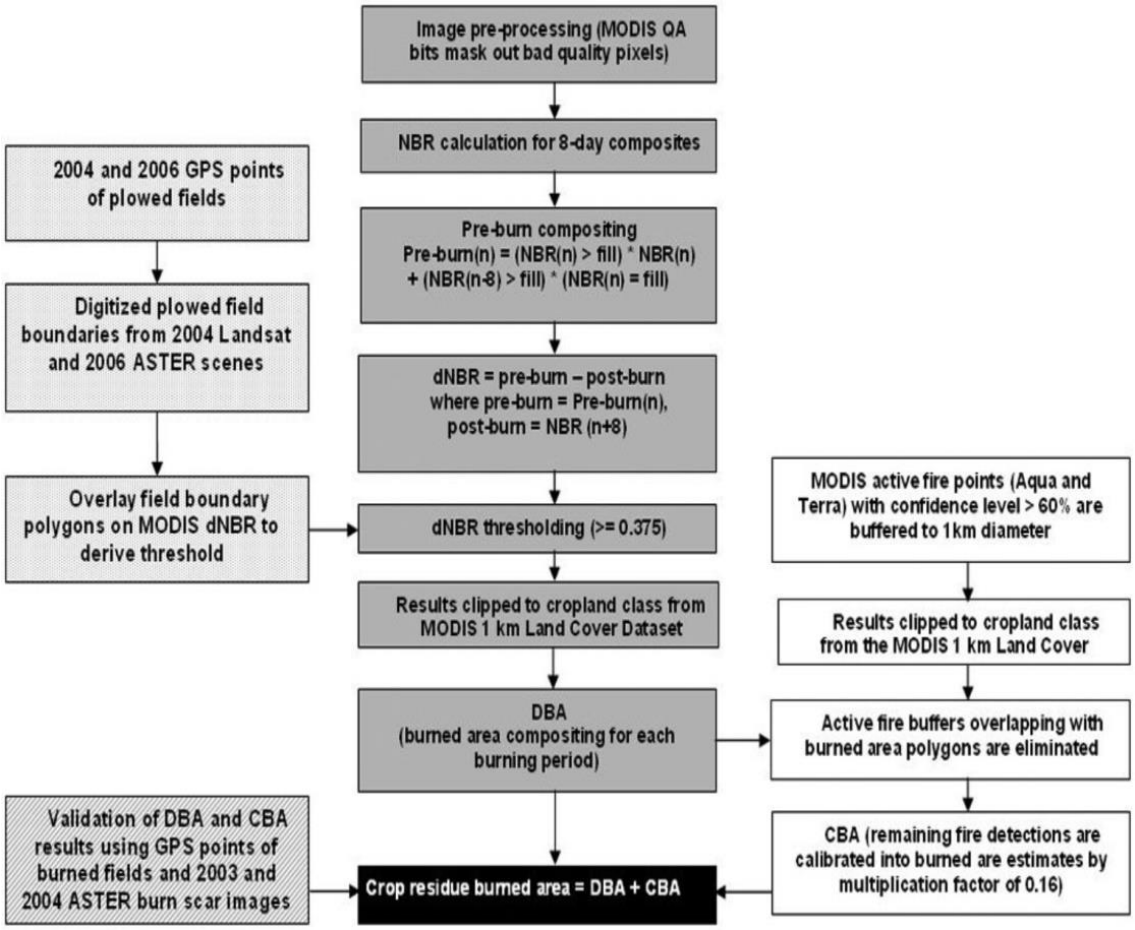

Fig.1. Description of data processing and burned area algorithm for croplands DBA = dNBR burned area product, CBA = Calibrated active fire burned area product (Taken from McCarty *et al.* 2008).

The combination of calibrated active fire points with dNBR area product proved to be important as the two products provided complementary information. The active fire points calibrated into burned area only contributed <4% of the total burned area detected using the hybrid approach but, despite a small overall contribution to the areal estimates, they identified spatial patterns that the dNBR burned area product omitted. Approximately 70% of the active fire detects were in areas not overlapping the dNBR burned area, demonstrating that even with small contribution to area, the active fire product was able to detect those smaller fires that the MODIS dNBR product, with 500-m^2 resolution, was unable to detect. The MODIS dNBR, likewise, is able to provide information on burned area that the calibrated active fire product omitted. Since active fire algorithm is only able to detect an actively burning fire during the time of overpass, and because of cloud cover potentially obscuring the view at the overpass time, there is potential for missed detections. The MODIS dNBR product has the ability to detect fires that occur in between overpasses due to the persistence on the ground of the spectral changes due to the fire (e.g. removal of the agricultural residue, soil exposure and deposition of charcoal).

Due to the fact that the McCarty (2008) approach was not systematically applied outside the United States, and was not available for other regions (Huang *et al.* 2012), subsequent studies did not use any burned area product, and relied uniquely on MODIS Terra and Aqua active fire detection (Korontzi *et al.* 2008; Vadrevu *et al.* 2011)..

Uncertainties and Conclusion

While the MODIS active fire product is effective at displaying spatial and temporal patterns of cropland fire events (Giglio *et al.* 2003; Giglio *et al.* 2006; Korontzi *et al.* 2006), the simple accumulation of active fire counts can lead to a significant bias in the areal

estimates, and in turn under- or over-estimate cropland residue fire emissions (Giglio *et al.* 2006; McCarty *et al.* 2008).

The MODIS system is able to detect only a subset of active fires due to the limited temporal sampling (typically four overpasses a day): agricultural fires are usually short lived, and might not be actively burning at the 10:30 am and 1:30 pm overpass time of Terra and Aqua respectively. Cloud and smoke obstructions decrease even further the detection rate. Secondly, the number of active fire counts is not immediately translated to agricultural burned area estimates. Strong correlation was shown for specific events, or specific regions (McCarty *et al.* 2008; McCarty *et al.* 2009; McCarty 2011), but do not immediately translate to valid correlation coefficients at the continental and global scale (Kasischke *et al.* 2003; Romanenkov *et al.* 2014).

The integration of dNBR and active fire products provide a more comprehensive estimate for burned area in cropland landscapes. However, the published methods were developed for regional applications, and caution must be taken when applying them outside those regions. The thresholds proposed by McCarty *et al.* (2008) would not be appropriate outside the study area, due to the variability of pre-fire and post-fire spectra. Soils properties, soil moisture, agricultural practices like irrigation or tillage, and fragmentation need to be accounted for each specific study area before the methodology can be applied. Field observations are therefore essential to apply this method to new areas.

Cropland residue fires are common in agricultural intensive regions and will become more common as the need for agricultural land use increases. As a large inter-annual variability exists for agricultural fires, the importance of developing a method for direct monitoring is stressed (McCarty *et al.* 2008). MODIS provides data with high temporal

resolution making it very ideal for monitoring agricultural landscapes for fire occurrence. The indirect approaches for monitoring fire, as presented and outlined from the reviewed literature in this paper, can easily over- or under-estimate burned area and therefore cropland residue fire emissions. A direct method for observing cropland fire would allow for development of spatially explicit and temporally dynamic models of emissions and air quality estimates for a growing number of users in the management and agricultural community (McCarty *et al.* 2008).

Table 3. Summary of studies that evaluated the use of MODIS for mapping agricultural fire

Acronyms used are as follows: MODIS, Moderate Resolution Imaging Spectroradiometer; ASTER, Advanced Spacebone Thermal Emission and Reflection Radiometer; AOD, aerosol optical depth; dNBR, differenced Normalized Burn Ratio; AWiFS, Advanced Wide Field Sensor

Study	Region	MODIS fire data approach	Validation	Results
Korontizi *et al.* (2006)	Global assessment	1-km MODIS (from Terra only) active fire product (MOD 14) used to estimate agricultural fire characteristics	Seasonal and interannual trends of agricultural fire activity is compared with known national and regional practices and crop production estimates	Total number of global agricultural fires are detected for years 2001-2003 Seasonal peaks are detected during April to May and August Russian Federation is identified as largest contirubutor to agricultural burning Active fire products are found consistent with known national and regional practices
McCarty *et al.* (2006)	Southeastern, USA	1-km MODIS (from Terra only) active fire product (MOD 14) used to estimate agricultural fire characteristics	n/a	Agricultural fire found as significant contributor to fire activity in southeastern US (16% of burning) Southeastern US contriubutes 33% of all cropland fire in the US Crop type, preperation and harvest practice affect the spatial and temporal variability of fire detections
Venkataraman *et al.* (2006)	Forests, Shrublands, and croplands, India	1-km MODIS (from Terra only) active fire product (MOD 14) used to estimate agricultural fire characteristics	Field observations/experience	Active fire products may be useful for capturing the seasonal variability of cropland fire May not be relaiable for burned area Open biomass burning emissions are estimated for 1995-2000
McCarty *et al.* (2008)	Southern Great Plains, southeastern USA	500-m MODIS 8-day surface relfectance product (MOD09A1) combined with 1-km MODIS active fire product (MOD14/MYD14) MOD09A1 used to derive dNBR for burned area.	Detected burned area was compared with in-situ and 15-m ASTER burnscar data	ASTER from 2003-2004 images show dNBR derived product slightly overestimates burned area (slope = 1.03 R^2=0.92, n=58) for 2003 and (slope=1.06, R^2=0.93, n=43) for 2004 Field data shows agreement (n=21, Kappa = 0.79) for 2004 and (n=48, Kappa = 0.89) for 2006
Korontizi *et al.* (2008)	Mississippi River Valley region, southeastern USA	1-km MODIS active fire product (MOD 14/MYD14) used to estimate agricultural fire characteristics	Accuracy assessment performed using coincident 30-m active fire observations from ASTER data.	Smallest flaming (800-1000K) fire size detectable at 50% probability with MODIS is 100m² Strong diurnal signal was detected during fall months No diurnal varaition in spring months.
McCarty *et al.* (2009)	CONUS	500-m MODIS 8-day surface relfectance product (MOD09A1) combined with 1-km MODIS active fire product (MOD14/MYD14) MOD09A1 used to derive dNBR for burned area.	Total of 296 GPS points including in-situ data about field sample were collected. In-situ data digitized using 15-m ASTER, 30-m Landsat TM, and 56-m AWiFS	In general, regions displayed agreement between 500-m dNBR product and in-situ field boundary data (78%-90%) provides mean annual burned agricultural area (2003-2007)
Vadrevu *et al.* (2011)	Indo-Ganges region, India	1-km MODIS active fire product (MOD 14/MYD14) used to estimate agricultural fire characteristics	n/a	Provides mean AOD for 2003-2008 Increased AOD coincided well with winter argicultral fires but weak relationship with summer agircultural fires
McCarty (2011)	CONUS	500-m MODIS 8-day surface relfectance product (MOD09A1) combined with 1-km MODIS active fire product (MOD14/MYD14) MOD09A1 used to derive dNBR for burned area	Detected burns were compared to in-situ, 15-m ASTER, 30-m Landsat TM, and 56-m AWiFS data	Provides average annual (2003-2007) emissions from crop residue burning for CONUS CO and CH4 emissions from crop residue burning by EPA were 73 and 78% higher than the emission estimates from anaylsis Accuracy of burned area mapping of 84%.
Huang *et al.* (2012)	Rural agricultral and peri-urban areas, China	1-km MODIS active fire product (MOD14/MYD14) used to estimate agriculturalfire characteristics	n/a	Provides average annual (2003-2010) emissions from crop residue burning for China North China Plain, Northeast China, and South China are main contributors to emissions from agircultural open burning Emissions are significantly associated with local sowing and harvest seasons.

References

Andreae, MO, Merlet, P (2001) Emission of trace gases and aerosols from biomass burning. *Global biogeochemical cycles* **15**, 955-966.

Aneja, VP, Schlesinger, WH, Nyogi, D, Jennings, G, Gilliam, W, Knighton, RE, Duke, CS, Blunden, J, Krishnan, S (2006) Emerging national research needs for agricultural air quality. *Eos, Transactions American Geophysical Union* **87**, 25-29.

Bond, TC, Doherty, SJ, Fahey, D, Forster, P, Berntsen, T, DeAngelo, B, Flanner, M, Ghan, S, Kärcher, B, Koch, D (2013) Bounding the role of black carbon in the climate system: A scientific assessment. *Journal of Geophysical Research: Atmospheres* **118**, 5380-5552.

Canode, C, Law, A (1979) Thatch and tiller size as influenced by residue management in Kentucky bluegrass seed production. *Agronomy journal* **71**, 289-291.

Crutzen, PJ, Andreae, MO (1990) Biomass burning in the tropics: Impact on atmospheric chemistry and biogeochemical cycles. *Science* **250**, 1669-1678.

Csiszar, IA, Morisette, JT, Giglio, L (2006) Validation of active fire detection from moderate-resolution satellite sensors: the MODIS example in northern Eurasia. *Geoscience and Remote Sensing, IEEE Transactions on* **44**, 1757-1764.

Davies, DK, Ilavajhala, S, Wong, MM, Justice, CO (2009) Fire information for resource management system: archiving and distributing MODIS active fire data. *Geoscience and Remote Sensing, IEEE Transactions on* **47**, 72-79.

Dennis, A, Fraser, M, Anderson, S, Allen, D (2002) Air pollutant emissions associated with forest, grassland, and agricultural burning in Texas. *Atmospheric Environment* **36**, 3779-3792.

Feng, N, Christopher, SA (2013) Satellite and surface-based remote sensing of Southeast Asian aerosols and their radiative effects. *Atmospheric Research* **122**, 544-554.

Friedl, MA, McIver, DK, Hodges, JCF, Zhang, XY, Muchoney, D, Strahler, AH, Woodcock, CE, Gopal, S, Schneider, A, Cooper, A, Baccini, A, Gao, F, Schaaf, C (2002) Global land cover mapping from MODIS: algorithms and early results. *Remote sensing of environment* **83**, 287-302.

Garcia, ML, Caselles, V (1991) Mapping burns and natural reforestation using Thematic Mapper data. *Geocarto International* **6**, 31-37.

Giglio, L (2010) MODIS Collection 5 Active Fire Product User's Guide Version 2.4.

Giglio, L, Descloitres, J, Justice, CO, Kaufman, YJ (2003) An enhanced contextual fire detection algorithm for MODIS. *Remote sensing of environment* **87**, 273-282.

Giglio, L, Kendall, J, Justice, C (1999) Evaluation of global fire detection algorithms using simulated AVHRR infrared data. *International Journal of Remote Sensing* **20**, 1947-1985.

Giglio, L, Van der Werf, G, Randerson, J, Collatz, G, Kasibhatla, P (2006) Global estimation of burned area using MODIS active fire observations. *Atmospheric Chemistry and Physics* **6**, 957-974.

Hawbaker, TJ, Radeloff, VC, Syphard, AD, Zhu, Z, Stewart, SI (2008) Detection rates of the MODIS active fire product in the United States. *Remote sensing of environment* **112**, 2656-2664.

Huang, X, Li, M, Li, J, Song, Y (2012) A high-resolution emission inventory of crop burning in fields in China based on MODIS Thermal Anomalies/Fire products. *Atmospheric Environment* **50**, 9-15.

Huete, A., Justice, C., & Van Leeuwen, W. (1999). MODIS vegetation index (MOD13). Algorithm theoretical basis document, 3, 213.

Justice, C. O., Vermote, E., Townshend, J. R., Defries, R., Roy, D. P., Hall, D. K., ... & Barnsley, M. J. (1998). The Moderate Resolution Imaging Spectroradiometer (MODIS): Land remote sensing for global change research. *Geoscience and Remote Sensing, IEEE Transactions on*, 36(4), 1228-1249.

Justice, C, Giglio, L, Korontzi, S, Owens, J, Morisette, J, Roy, D, Descloitres, J, Alleaume, S, Petitcolin, F, Kaufman, Y (2002) The MODIS fire products. *Remote sensing of environment* **83**, 244-262.

Kasischke, ES, Hewson, JH, Stocks, B, van der Werf, G, Randerson, J (2003) The use of ATSR active fire counts for estimating relative patterns of biomass burning–a study from the boreal forest region. *Geophysical Research Letters* **30**.

Kaufman, YJ, Justice, CO, Flynn, LP, Kendall, JD, Prins, EM, Giglio, L, Ward, DE, Menzel, WP, Setzer, AW (1998) Potential global fire monitoring from EOS-MODIS. *Journal of Geophysical Research: Atmospheres (1984–2012)* **103**, 32215-32238.

Kaufman, YJ, Setzer, A, Justice, C, Tucker, C, Pereira, M, Fung, I (1990) Remote sensing of biomass burning in the tropics. In 'Fire in the Tropical Biota.' pp. 371-399.

Korontzi, S, McCarty, J, Justice, C (2008) Monitoring agricultural burning in the mississippi River Valley Region from the moderate resolution imaging spectroradiometer (MODIS). *Journal of the Air & Waste Management Association* **58**, 1235-1239.

Korontzi, S, McCarty, J, Loboda, T, Kumar, S, Justice, C (2006) Global distribution of agricultural fires in croplands from 3 years of Moderate Resolution Imaging Spectroradiometer (MODIS) data. *Global biogeochemical cycles* **20**, 1-15.

Lamb, P, Murray, G (1999) Kentucky bluegrass seed and vegetative responses to residue management and fall nitrogen. *Crop science* **39**, 1416-1423.

Loveland, T, Belward, A (1997) The IGBP-DIS global 1km land cover data set, DISCover: first results. *International Journal of Remote Sensing* **18**, 3289-3295.

Leff, B, Ramankutty, N, Foley, JA (2004) Geographic distribution of major crops across the world. *Global biogeochemical cycles* **18**.

McCarty, J, Justice, C, Korontzi, S (2007) Agricultural burning in the Southeastern United States detected by MODIS. *Remote sensing of environment* **108**, 151-162.

McCarty, J, Loboda, T, Trigg, S (2008) A hybrid remote sensing approach to quantifying crop residue burning in the United States. *Applied Engineering in Agriculture* **24**, 515-527.

McCarty, JL (2011) Remote sensing-based estimates of annual and seasonal emissions from crop residue burning in the contiguous United States. *Journal of the Air & Waste Management Association* **61**, 22-34.

McCarty, JL, Ellicott, EA, Romanenkov, V, Rukhovitch, D, Koroleva, P (2012) Multi-year black carbon emissions from cropland burning in the Russian Federation. *Atmospheric Environment* **63**, 223-238.

McCarty, JL, Korontzi, S, Justice, CO, Loboda, T (2009) The spatial and temporal distribution of crop residue burning in the contiguous United States. *Science of the total environment* **407**, 5701-5712.

Melvin, M (2012) National prescribed fire use survey report.

Romanenkov, V, Rukhovich, D, Koroleva, P, McCarty, JL (2014) Estimating Black Carbon Emissions from Agricultural Burning. In 'Novel Measurement and Assessment Tools for Monitoring and Management of Land and Water Resources in Agricultural Landscapes of Central Asia.' pp. 347-364.

Roy, D, Jin, Y, Lewis, P, Justice, C (2005) Prototyping a global algorithm for systematic fire-affected area mapping using MODIS time series data. *Remote sensing of environment* **97**, 137-162.

Roy, D, Lewis, P, Justice, C (2002) Burned area mapping using multi-temporal moderate spatial resolution data—A bi-directional reflectance model-based expectation approach. *Remote sensing of environment* **83**, 263-286.

Running, S, Justice, C, Salomonson, V, Hall, D, Barker, J, Kaufmann, Y, Strahler, A, Huete, A, Muller, J-P, Vanderbilt, V (1994) Terrestrial remote sensing science and algorithms planned for EOS/MODIS. *International Journal of Remote Sensing* **15**, 3587-3620.

Sharma, AR, Kharol, SK, Badarinath, K (2009) Satellite observations of unusual dust event over North-East India and its relation with meteorological conditions. *Journal of Atmospheric and Solar-Terrestrial Physics* **71**, 2032-2039.

Smith, P, Gregory, PJ, Van Vuuren, D, Obersteiner, M, Havlík, P, Rounsevell, M, Woods, J, Stehfest, E, Bellarby, J (2010) Competition for land. *Philosophical Transactions of the Royal Society B: Biological Sciences* **365**, 2941-2957.

Vadrevu, KP, Ellicott, E, Badarinath, K, Vermote, E (2011) MODIS derived fire characteristics and aerosol optical depth variations during the agricultural residue burning season, north India. *Environmental Pollution* **159**, 1560-1569.

Venkataraman, C, Habib, G, Kadamba, D, Shrivastava, M, Leon, JF, Crouzille, B, Boucher, O, Streets, DG (2006) Emissions from open biomass burning in India: Integrating the inventory approach with high-resolution Moderate Resolution Imaging Spectroradiometer (MODIS) active-fire and land cover data. *Global biogeochemical cycles* **20**, GB2013.

Wolfe, R., Roy, D., Vermote, E., (1998), The MODIS land data storage, gridding and compositing methodology: L2 Grid, IEEE Transactions on Geoscience and Remote Sensing, 36:1324-1338

Yevich, R, Logan, JA (2003) An assessment of biofuel use and burning of agricultural waste in the developing world. *Global biogeochemical cycles* **17**

Chapter 2: Characterization of the Spectral Signature of Agricultural Burned Areas[1]

Abstract

Timely and accurate assessments of the extent and location of agricultural fires are needed to correctly quantify their contribution to global fire emissions and also to assist decision makers involved in human health and air quality regulations at the local level. Previous works have shown that spectral signatures of cropland burned areas and bare soil are relatively indistinguishable resulting in significant detection uncertainty from corresponding remote sensing products. The present evaluates burned area mapping spectral indices applied toLandsat 8 OLI data for various cropland pixel mixtures by monitoring the spectral signal throughout the harvest, burning and tilling periods. The field data collection was conducted in the east-central Palouse region of northwestern Idaho and southeastern Washington. Surface reflectance was measured on experimental plots of spring wheat and barley fields with an Analytical Spectral Device (ASD) FieldSpec Pro radiometer following the VALERI protocol for upscaling the field measurements to 30 meter pixels (Baret *et al.* 2005). All the dates for field data collections are coincident with Landsat 8 OLI overpasses. Mixture models were used to simulate Landsat pixel signatures for various mixtures of post-harvest agricultural residue with exposed wet/dry soil or burned agricultural residue. Results show minimal separation exists between model outputs for mixtures containing post-harvest residue with burned residue and post-harvest residue with exposed wet/dry soils. The results of this research indicate that reliable detection of burned area in agricultural regions cannot be

[1] Article submitted to the International Journal of Wildland Fire (2015)

performed with the conventional spectral index approaches, unless full combustion occurs for the entire area of the target pixel.

Introduction

Quantifying the temporal and spatial variability of cropland burning is needed to improve our understanding for creating precise emission inventories and develop informed legislative measures to mitigate the contribution to air pollution (Aneja *et al.* 2006). Past studies have demonstrated the potential application of satellite remote sensing data to produce temporal and spatial statistics of biomass burned from prescribed agricultural fires (McCarty *et al.* 2007; McCarty 2011; Huang *et al.* 2012). Large uncertainties caused by ambiguous spectral features and temporal patterns of cropland fires, however, still hinder the development of global products that can be used for local policy and management applications (Roy *et al.* 2008; Randerson *et al.* 2012).

The Moderate Resolution Imaging Spectroradiometer (MODIS) system, aboard the polar orbiting EOS-AM1 (Terra) and EOS-PM1 (Aqua) satellites of the National Aeronautics and Space Administration (NASA) Earth Observing System (EOS), was the first sensor specifically designed with dedicated bands for fire detection (Kaufman *et al.* 1998). These sensors provide at a global scale two observations during the day and two at night. Two fire products are part of the suite of thematic land products, available systematically for the duration of the mission (year 2000 onward): the MOD/MYD14 1-km global active fire product (Justice *et al.* 2002; Giglio *et al.* 2003) and the MCD45A1 500-m global burned area product (Roy *et al*, 2005; Roy *et al.* 2008). A more detailed description of the MODIS fire products used for agricultural burned area detection is presented in chapter 1.

As discussed in the previous chapter, both the MOD/MYD 14 active fire and MCD45A1 burned area detection products have limitations in their ability to monitor agricultural fires. The MOD/MYD14 detection rate is negatively affected by the widespread presence of quick burning cropland fires that occur at times other than overpass. As a combination of the fast temporal dynamic of cropland fires and their low biomass load, the amount of energy required for the active fire detection is often not released at the time of satellite overpass, even if the fire is actively burning. Detection rates have been also shown to be affected by the presence of heavy smoke or cloud cover (Csiszar *et al.* 2006; Hawbaker *et al.* 2008). In case of an active fire detection, the binary (fire/not fire) nature of the algorithm does not allow for a direct estimate of the actual area burned within the 1-km active pixel (Kasischke *et al.* 2003; Giglio *et al.* 2006; Romanenkov *et al.* 2014).

The MCD45A1 burned area product also has severe limitations for cropland burned area detection. Information provided by this product has indicated that ~1.3% of global cropland area was burned from 1997-2010 (Giglio *et al.* 2010) and that this is most likely an underestimation as many cropland fields and fires are much smaller than the 25-ha surface reflectance pixel (Roy *et al.* 2008; Lin *et al.* 2012). Furthermore, the temporal persistence of agricultural burned areas is often shorter than the minimum persistence time requested by the MCD45A1 algorithm: in many cases, burning is immediately followed by plowing, with as little as a single day between the two events. Although the product's use is sometimes unavoidable, the combination of these two effects can lead to a significant underestimation of the total agricultural burned area, and makes MCD45A1 unsuitable as the primary data sources for studying burned areas in agricultural landscapes (J.L. McCarty, Michigan Tech Research Institute, personal communication).

The United States Geological Survey (USGS) has been distributing Landsat data at no charge via the internet since 2008 (Woodcock *et al.* 2008), allowing for unprecedented opportunities for long-term and large-scale environmental monitoring at the 30 meter scale, including systematic burned area mapping (Boschetti *et al*. 2015). There are advantages and limitations in the potential use of Landsat for mapping agricultural burned areas. The high spatial resolution (30-m) is compatible with the typical size of agricultural fields, but the low temporal resolution (16 day revisit time) can be problematic when agricultural practices include rapid tilling of the burned areas. For example, a field may progress from post-harvest agricultural residue to burned residue and then to tilled soil between Landsat overpass periods. By missing this progression, it would be impossible to know whether the field was burned and then tilled or if the field was only tilled.

Even at the Landsat scale some heterogeneity remains, due to pixel mixing caused by weathering, management effects and the terrain's heterogeneous nature (Watts *et al.* 2009). In order to avoid commission errors from other forms of land cover or land cover change (harvesting or tilling), most burned area algorithms will require a large fraction of an individual pixel's area to undergo a complete burn event in order for detection to be successful (Roy and Boschetti 2009; Randerson *et al.* 2012). Roy and Landmann (2005) have addressed the problem of mixed pixels by developing a specific mixture model for burned areas.

The objective of the paper are to evaluate whether linear and non-linear spectral mixture models provide any improvement over common burned area spectral indices in identifying agricultural burned areas when applied to Landsat data on an agricultural region where cropland burning is a common management practice.

Methods

a. Study Area

The study was conducted in the east central Palouse Prairie region. The Palouse bioregion covers 16,000-km^2 in southeastern Washington, west central Idaho, and northeastern Oregon (Bailey 1995). The region is characterized by hot, dry summers followed by wet and relatively warm winters. The east central Palouse region was once a widespread prairie composed of perennial grasses such as Blue bunch wheatgrass (*Psuedoregneria Spicata*) and Idaho fescue (*Festuca idahoensis*). Today it is virtually all planted in agricultural crops (Black *et al.* 1998).With a rolling landscape of mostly developed loess hills, soils are often more than 100-cm deep giving the region some of the world's most fertile soils for producing cereal crops such as wheat and barley (Williams 1991).

For the collection of pre- and post-harvest agricultural residue measurements, study sites were selected at two primary locations east of Genesee Idaho, USA while exposed soil and burned agricultural residue endmember measurements were collected in separate sites west of Potlatch Idaho, USA (Fig. 2). Pre-harvest ground measurements are not presented here, but were used to compare to satellite data.

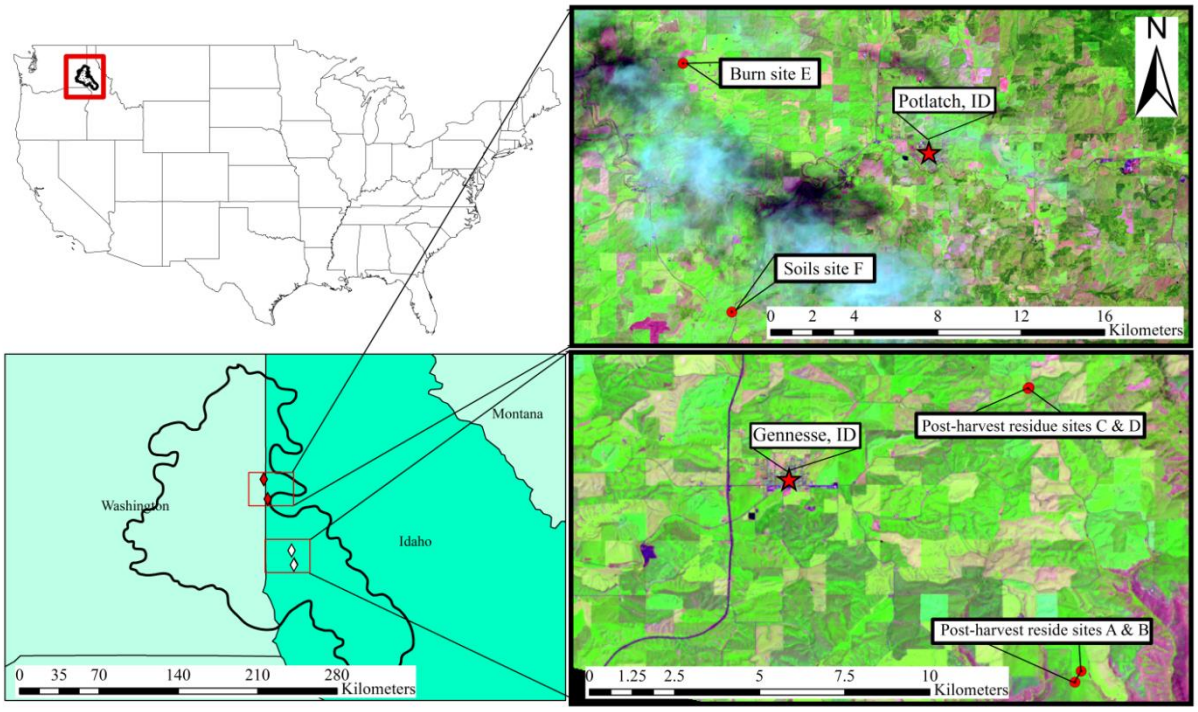

Fig.2 Palouse bioregion outlined in the inland northwest, USA (top left). Locations of primary sites A- D illustrated as white diamonds and burned/soil land cover spectral data collection sites illustrated as red diamonds (bottom left). Close up of site A and B overlaid on individual Landsat 8 OLI pixels of interest in false composite: R: SWIR 1.5 (1.57-1.65 µm) G: NIR (0.85-0.88 µm) B: Red (0.64-0.67 µm) (right).

This study adapted methods from the VALERI field campaign in order to upscale our site field measurements to a single 30x30-m Landsat 8 OLI pixel (Baret *et al.* 2005). Sites contained two center-crossed 30-m transects with sample locations occurring every 5-m in addition to each of the corners, totaling 17 samples per site. The precise position of each site was pre-determined by selecting Landsat 8 OLI pixels in cropland areas that were relatively flat and homogenous crops. The geographic coordinates of the selected pixels were located in the field and the center-crossed transects were arranged on the precise location based on the

center-pixel coordinates retrieved from the downloaded Landsat 8 OLI scene. Selected plot metadata describing characteristics of each site are summarized in (Table 4). The field sites were specifically selected areas free of interference from man-made objects (e.g. power lines, roads, etc.). The cereal crops were chosen due to their abundance in the Palouse and for the regularity of post-harvest biomass residue burning as a management practice. Ground data was collected during the Landsat 8 OLI overpass immediately following harvest (within eight days). For a more detailed description of the VALERI protocol, refer to the appendix at the end of this document.

Table 4. Plot crop type and ancillary data

Site	Crop/Land cover type	Center pixel coordinates (decimal degrees)	Elevation (m)	Date of sample collection
A	Spring wheat (Hard white)	46.498390 N, 116.816900 W	768	August 2nd
B	Barley	46.500271 N, 116.816122 W	749	August 11th
C	Spring wheat (Hard red)	46.576164 N, 116.833084 W	879	August 27th
D	Spring wheat (Hard red)	46.575897 N, 116.833481 W	871	August 27th
E	Burned agricultural reside	46.962334 N, 117.053902 W	773	September 11th
F	Exposed soil	46.855170 N, 117.024664 W	821	September 11th/ December 8th

Burned agricultural endmembers were collected within a day of each prescribed fire. Dry soil measurements were collected on the same day, at the end of the dry season. Because of the weather pattern in the Palouse it was not possible to collect wet soil measurements for the whole summer; the measurements were collected instead in late fall, after a long period of precipitation.

Soil and burn measurements were made at separate sites because it was not possible to locate a field that had the definite expectation of later burning or tilling after harvest due to

the unpredictable nature of management practice based off of field conditions. Access was granted for repeated sampling of sites A-D while the burn and soil sites were later chosen for their similar landscape, crop types and seasonal spectral profile. Given this information, it is reasonable to assume that the averaged measurements of sites A-D are an adequate characterization of pre-fire conditions of cereal crops in the study area. The burn sites were located using local MOD14/MYD14 active fire detections. No prescribed fire data (including fire or tilling management data) was collected.

b. Data

Spectral ground measurements were made using an Analytical Spectral Devices (ASD) FieldSpec Pro with a spectral range of 350-2500 nm and 1.4-nm sampling interval (Analytical Spectral Devices, Boulder, Colorado, USA). A hand-held wand device was designed and built to house the pistol grip and fore-optic 0.5 m away from the researcher to minimize shadow or object interference. The cable fore-optic has a field of view of 25°. Measurements were taken from the nadir viewing angle, 0.5 m above canopy. Sampling occurred in the direction of solar irradiance to minimize the effects of bi-directional reflectance uncertainty.

ASD spectral reflectance data was converted into the band equivalent reflectance of Landsat 8 OLI bands 1-8 through a convolution process using a suite of relative spectral response functions for each ground collection (Trigg and Flasse 2001; Smith *et al.* 2005). The 17 samples were then averaged across the plot to estimate the spectral signature of the Landsat 8 OLI pixel. For the present study, four spectral endmembers are considered: unburned agricultural residue, dry soil (post-tilling), wet soil (post-tilling), burnt agricultural residue. Each endmember was estimated by upscaling the 17 ground collected spectral

samples at the corresponding ground plot. The averaged endmembers were used as input data for the mixture modeling phase of the study. Wet (saturated) soil was considered a unique endmember given patches of standing water were not a realistic component of the Landsat 8 OLI pixels.

All collections, including measurements for determining burned agricultural residue endmembers, were coincident with Landsat 8 OLI overpasses during clear and sunny local weather conditions. A more detailed description of the Landsat 8 OLI data set can be found at the end of this document (See Appendix).

c. Mixture Modeling

Two modeling approaches were used to simulate a variety of mixtures of land cover within a Landsat 8 OLI pixel. Following Roy and Landmann (2005) we simulated the spectral response of varying pixel mixtures of unburned post- harvest and burned agricultural residue as a function of combustion completeness and fraction of observed land cover area that burned within the pixel (Eq. 1). The second approach is a simple linear mixture model (Eq. 2) which was used to simulate the spectral response of varying pixel mixtures of unburned post-agricultural residue with exposed soil surface (wet and dry) as a function of the fraction observed soil land cover area in the pixel.

$$\rho_t = (1 - fcc)\rho_u + fcc\rho_b \quad (1)$$

$$\rho_t = (1 - f)\rho_u + f\rho_s \quad (2)$$

Where ρ_t is the target reflectance of a mixed pixel, ρ_u is the unburned agricultural residue endmember input, ρ_b is the burned agricultural residue endmember input, ρ_s is the exposed

soil endmember input, f is the fraction of observed area (exposed soil or burned residue) ($0 < f < 1$) and cc is the combustion completeness ($0 < cc < 1$).

All model calculations were computed using the R statistical environment (R Development Core Team 2014). The normalized burn ratio (NBR = $\rho NIR-\rho SWIR_{2.1}/\rho NIR+\rho SWIR_{2.1}$) (Key and Benson 1999), normalized difference vegetation index (NDVI = $\rho NIR-\rho Red/\rho NIR+\rho Red$) (Rouse Jr *et al.* 1974) and mid-infrared burn index (MIRBI =$10\rho SWIR_{2.1}-9.8\rho SWIR_{1.5}+2$) (Trigg and Flasse 2001) were selected as the spectral indices of interest. The spectral indices selected in this study have been widely applied in burned area detection in non-forested ecosystems (e.g., savannahs, grasslands, and sage-steppe), which given the non-vertical canopy nature of agricultural fields was considered a reasonable analogue (Fraser *et al.* 2000; Domenikiotis *et al.* 2002; Escuin *et al.* 2007; Zhang and Kondragunta 2008). The spectral indices for post-harvest endmembers were calculated using averaged band values from sites A-D to simulate typical index values for post-harvest residue.

Results

The calculated endmembers gathered from the field campaign are presented (Table 5). Post-harvest values shown in figure 3 are calculated by averaging each channel value from sites A-D. Averaged post-harvest ground data did not appear to be inconsistent from typical Landsat 8 OLI measurements of post-harvest residue for cereal crops in the Palouse.

By applying equation (1) and (2) it is possible to simulate reflectance values and spectral indices of a mix of agricultural residue, burned residual, dry and wet soils. The spectral trajectories of the reflectance values, plotted as a function of the fraction of area

burned and combustion completeness and as a function of the exposed bare soil are presented in Figure 3. The corresponding trajectories for the spectral indices are presented in Figure 4.

Table 5. Spectral endmembers and burn indices considered. Values are derived from convolution of ASD ground data into Landsat 8 OLI surface reflectance values per band. Index values are calculated from averaged bands 4-7 surface reflectance values for sites A-D.

Land cover	Band 4	Band 5	Band 6	Band 7	NBR	MIRBI	NDVI
Averaged A-D	0.393469	0.543632	0.511143	0.328222	0.247072	0.273015	0.160243
Wet soil	0.048526	0.080429	0.136967	0.10843	-0.14827	1.742002	0.247391
Dry Soil	0.132128	0.185262	0.264224	0.240641	-0.13003	1.817009	0.167411
Burned	0.047826	0.070418	0.132904	0.13852	-0.32595	2.082741	0.191065

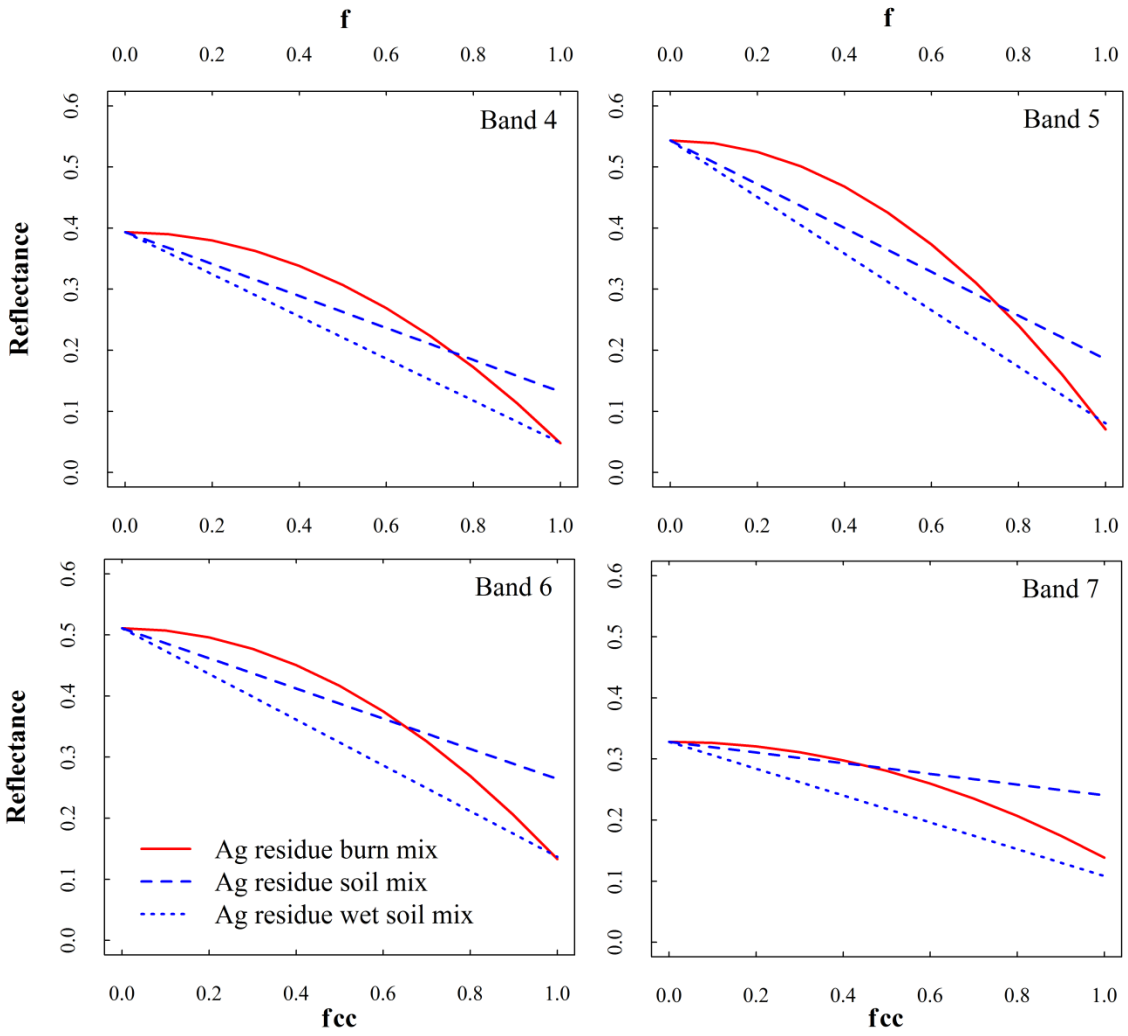

Fig.3. Mixture model trajectories for Landsat 8 OLI bands 4-7.The solid line represents the post-harvest agricultural residue and burned agricultural mix trajectory as a function of the

product of fraction of observed burned area and combustion completeness (f_{cc}) which is expressed on the bottom x-axis. The dashed line represents the post-harvest agricultural residue and dry soil mix trajectory as a function of the fraction of observed area of exposed soil (f) which is expressed on the top x-axis. The dotted line represents the post-harvest agricultural residue and wet soil mix trajectory as a function of the fraction of observed area of exposed soil (f) which is reported on the top x-axis.

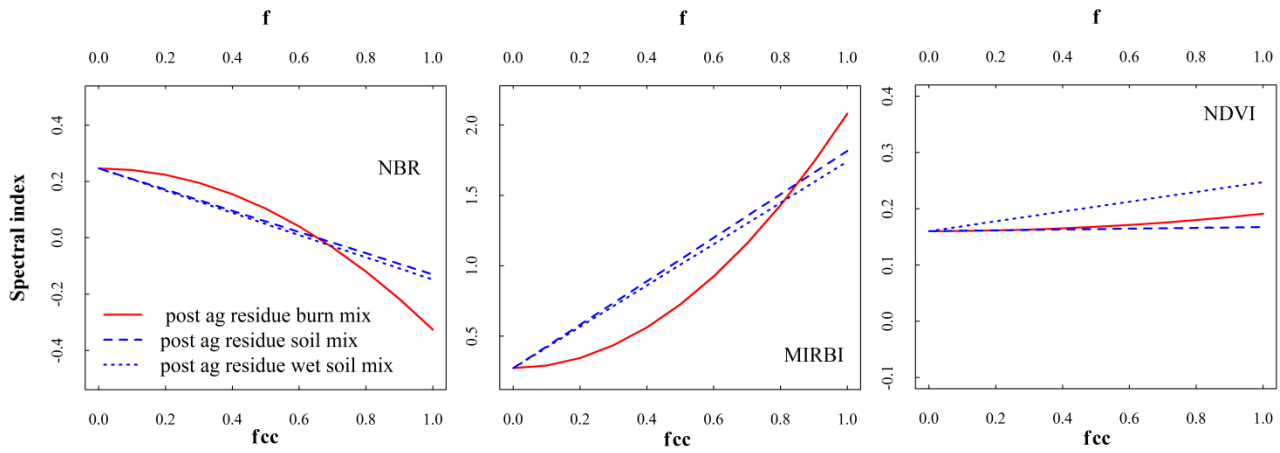

Fig. 4. Mixture model trajectories for Landsat 8 OLI burn indices. The solid line represents the post-harvest agricultural residue and burned agricultural mix trajectory as a function of the product of fraction of observed burned area and combustion completeness (f_{cc}) which is expressed on the bottom x-axis. The dashed line represents the post-harvest agricultural residue and dry soil mix trajectory as a function of the fraction of observed area of exposed soil (f) which is expressed on the top x-axis. The dotted line represents the post-harvest agricultural residue and wet soil mix trajectory as a function of the fraction of observed area of exposed soil (f) which is reported on the top x-axis.

The simulated spectral indices and bands 4-7 performed as expected, showing a reduction in reflectance as the surface transition from unburned agricultural residue to burned area, or to exposed soil. It should be noticed that, in all bands, the burned endmember and the wet soil endmember are extremely similar. Of the investigated indices, NDVI was wholly unsuitable, consistent with the literature on burned area mapping (Roy *et al*. 2005). Figure 4 highlights that, as post-harvest residue progresses to wet soil and burned residue, a slight increase in reflectance are observed potentially due to the presence of regenerating vegetation. All the other indices showed a good burned-unburned separation, but a poor separation between burned areas and soils. The burn residue spectral samples collected from the field included some soil and possibly very small amounts of left over senesced plant material. This follows what one would expect to see in reality since total combustion of the entire pixel area may never be the actual result of a cropland burn. In summary, all indices in figure 4 demonstrate minimal separation between burned areas and soils, indicating that the indices have poor performance if employed to map burned areas in cropland regions where both burning and tilling are common practices.

The upscaled ground spectral measurements were compared to the contemporaneous Landsat 8 OLI data, collected for each site's pixel at the time of the field measurements (Fig. 5 & 6). The figures demonstrated the temporal trajectory of the spectral values at each of the observed pixels throughout the growing season. In order to facilitate the interpretation of the trajectories, the bottom right quadrant of Figure 6 reports the land cover status for each site at each overpass date, and table 6 reports the harvest/burning/tilling dates.

All of the sites show a similar progression of spectral values throughout the growing season, with sharp increases in bands 4-7 immediately after harvest, with the exception of site

E. The increase in reflectance is consistent with the ground spectral measurements, and is due to dry, very reflective loose straw, almost completely covering the ground after harvest. The slight decrease in bands 4 and 5 for site E was only a local phenomenon as most of the neighboring pixels had increases in bands 4-7 during pre-harvest to post-harvest land cover change. No ground observations exist for site E immediately after harvest so it is not clear what may have caused the slight decrease in reflectance.

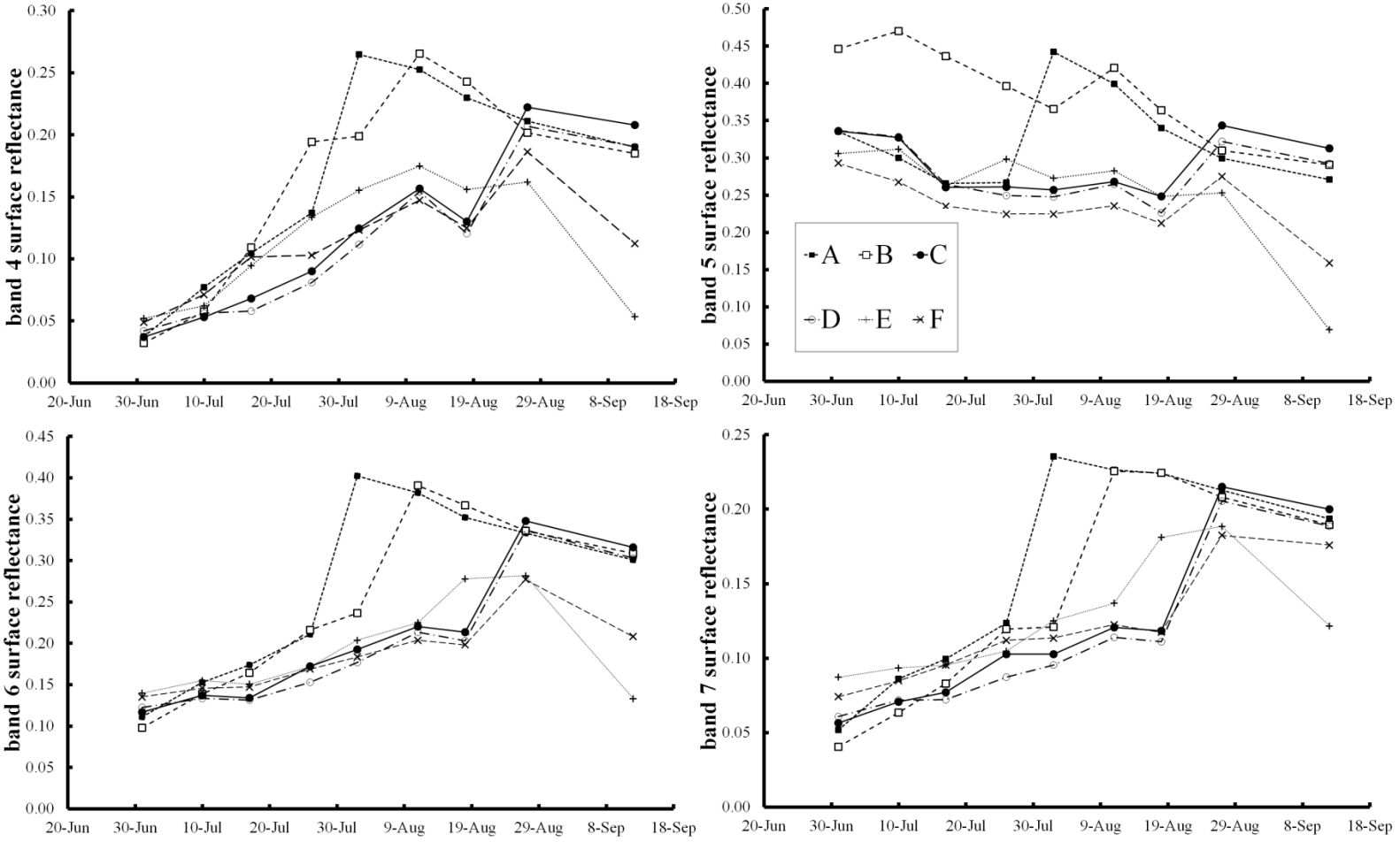

Fig. 5. Temporal profile of surface reflectance for bands 4-7 derived from nine Landsat 8 OLI overpass dates over the summer of 2014 for sites A-F throughout the growing, harvest, till and burning periods.

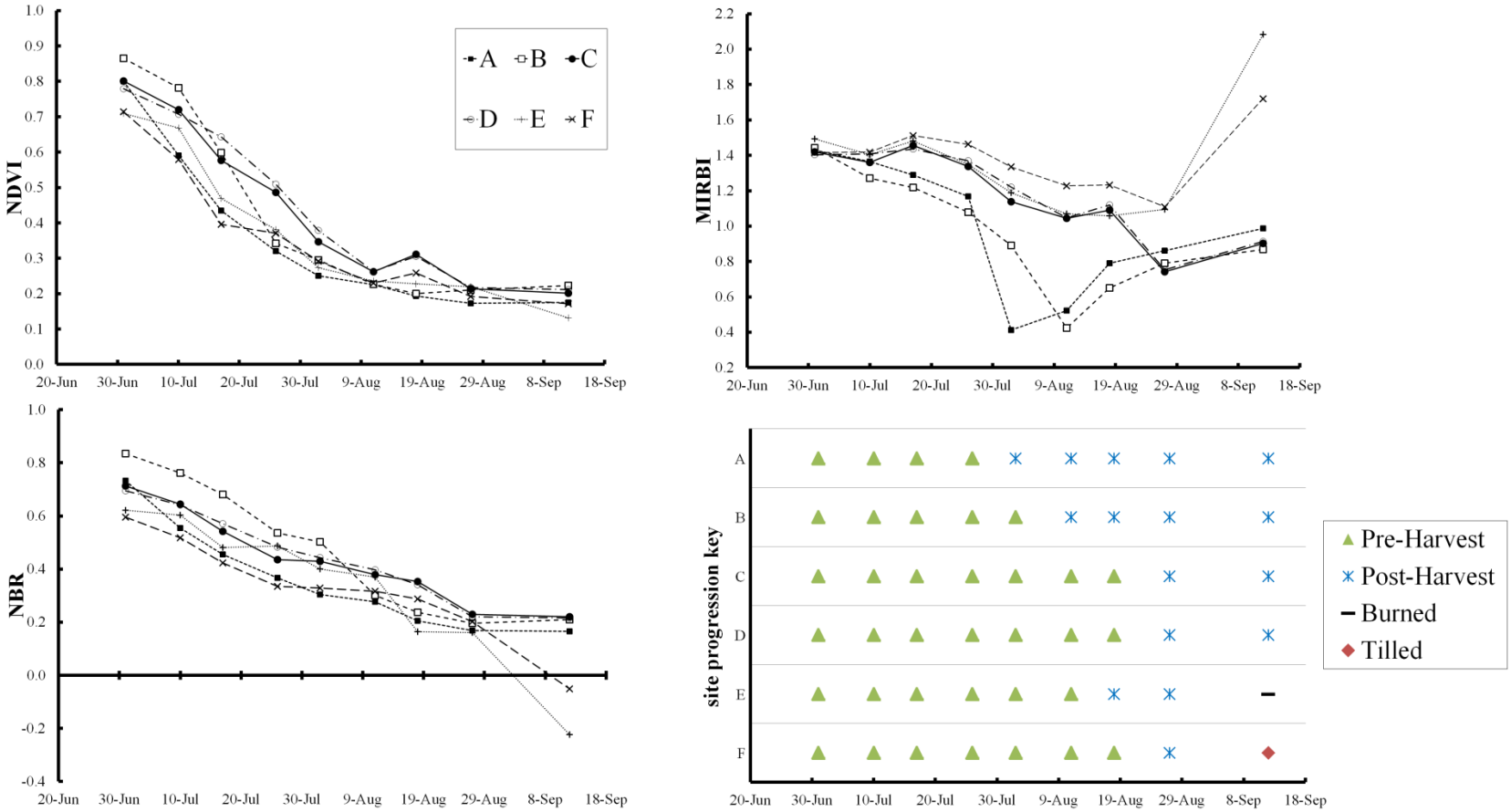

Fig. 6. Burn and vegetation spectral index temporal profiles derived from nine Landsat 8 OLI overpass dates over the summer of 2014 for sites A-F throughout the growing, harvest, till and burning periods. Site progression key (bottom right) illustrates the status of surface land cover.

Table 6. Date of first Landsat 8 OLI overpass after site surface cover change. Surface cover change type is listed.

Site	Harvest	Tilled	Burned
A	August 2	--	--
B	August 11	--	--
C	August 27	--	--
D	August 27	--	--
E	August 18	--	September 12
F	August 27	September 12	--

Consistent with the pattern observed in the mixture analysis of figure 4, figure 6 shows that the NDVI trajectories for burned and unburned sites are not separable. NBR performed slightly better as an index used for detecting changes caused by burning or tilling. Out of the three indices compared in figure 6, MIRBI provides the most explicit information for when a change occurs, with sharp decreases during harvesting and sharp increases during burning or tilling.

Reflectance values for all studied bands slowly decrease over time after harvest as loose straw is removed by the wind exposing the underlying soil. Plant matter decomposition and weathering may also play a role in the decrease of reflectance. This transformation is important to consider as it will affect the differenced index values between post-harvest residue and tilled or burned residue. For example, differencing averaged immediate post-harvest MIRBI from bare soil MIRBI results in a MIRBI value ~1.14. A near identical is produced (~1.17) after differencing September 12th post-harvest MIRBI from burned residue MIRBI, illustrating the temporal dimension of management practices effect on the indices ability to characterize burned area from tilled soil.

These channels and indices are also sensitive to the intrinsic variability of spectral signatures for soil and burned residue. The results from figure 3 and figure 4 illustrate that wet

soil is darker than dry soil in all the bands that were considered; thus lowering the probability of distinction in tilling and burning land cover changes. In addition to this, the burn residue included in this study was not calculated from a site that experienced a high-temperature fire, which occasionally occurs during prescribed cropland burning. High-temperature fires deposit white ash, which, if existing in sufficient quantities (e.g., >2% of a pixel), can act to reduce the total decrease in surface reflectance due to a burn event (Stronach and McNaughton 1989).

Conclusion

This study presented an original combination of ground data collection and spectral mixture models to investigate the spectral characteristics of agricultural burned areas. In particular, the study focused on understanding whether it is possible to reliably use spectral indices to detect agricultural burning, and to discriminate between agricultural burning and other agricultural practices such as tilling. Agricultural burned areas experience quick transitions from vegetation to soil or burned residue as an effect of management strategies, thus exhibiting temporal and spectral patterns very distinct from wildland fires. The study was conducted using six locations across the east-central portion of the Palouse region in western Idaho. Of these, four locations were used to characterize the spectral characteristics of post-harvest unburned residue, one for exposed soils following tilling, and one for burned residuals.

Spectral measurements of reflectance were performed using an ASD FieldSpec Pro instrument, and adopting the VALERI protocol (Baret *et al.* 2005). The ground sampling protocol allowed upscaling the measurements to the level of single Landsat pixels. Spectrally, the measurements were convoluted using the Landsat 8 OLI spectral response functions,

resulting in Landsat reflectances simulated from ground spectra. These simulated Landsat reflectances were used with the spectral mixture model proposed by Roy and Landmann (2005) to calculate the reflectance of mixed pixels as a function of the fractional cover of unburned residual, burned area and soil.

The results showed good separation of the NBR and MIRBI indices between unburned and burned spectra, but minimal separation between burned areas and soils, especially for low combustion completeness and fraction of area burned (f_{cc}). The NDVI index was instead insensitive to burning, showing in one case a slight increase.

The results provide an insight on the reasons why global burned area algorithms, usually designed to map wildfires (Roy *et al*. 2005), underperform over agricultural areas: with a low separability between the signal due to burning and the signal due to tilling, either commission errors (e.g. tilling mapped as burning) or omission errors (e.g. burning erroneously discarded as tilling) are inevitable.

Further research will target the specific problem of discriminating between the temporal trajectories of spectral indices caused by burning and tilling, and will include a comprehensive evaluation of the behavior of spectral indices, in particular investigating the potential of the joint use of several indices (Stroppiana *et al*. 2012).

Chapter 2 Acknowledgments

This project was supported through NASA and USDA funding. We thank Pietro Alessandro Brivio (CNR-IREA Istituto per il Rilevamento Electtromagnetico dell'Ambiente, Milano, Italy), Patrizia Arosio, Luca Marini and Andrea Melchoirre for assisting in the planning and execution of field data collection. We gratefully acknowledge the Odberg and Zenner Family

farms for granting access to their land to perform the spectral measurements throughout the season. We also thank Alistair Smith (University of Idaho) and Andrew Hudak (USDA Forestry Service) for use of Hemispherical and Spectral field equipment.

References

Aneja, VP, Schlesinger, WH, Nyogi, D, Jennings, G, Gilliam, W, Knighton, RE, Duke, CS, Blunden, J, Krishnan, S (2006) Emerging national research needs for agricultural air quality. *Eos, Transactions American Geophysical Union* **87**, 25-29.

Bailey, RG (1995) Description of the ecoregions of the United States. USDA Forest Service.

Baret, F, Weiss, M, Allard, D, Garrigues, S, Leroy, M, Jeanjean, H, Fernandes, R, Myneni, R, Privette, J, Morisette, J (2005) VALERI: a network of sites and a methodology for the validation of medium spatial resolution land satellite products. *Remote sensing of environment.*

Black, AE, Strand, E, Morgan, P, Scott, JM, Wright, RG, Watson, C (1998) Biodiversity and land-use history of the Palouse bioregion: pre-European to present. *Perspectives on the Land Use History of North America: A Context for Understanding Our Changing Environment. Biological Science Report. US Geological Survey, Biological Resources Division, Biological Science Report USGS/BRD/BSR–1998-0003* 85-99.

Boschetti, L., Roy, D. P., Justice, C. O., & Humber, M. L. (2015). MODIS–Landsat fusion for large area 30m burned area mapping. *Remote Sensing of Environment*, **161**, 27-42.

Csiszar, IA, Morisette, JT, Giglio, L (2006) Validation of active fire detection from moderate-resolution satellite sensors: the MODIS example in northern Eurasia. *Geoscience and Remote Sensing, IEEE Transactions on* **44**, 1757-1764.

Domenikiotis, C, Dalezios, NR, Loukas, A, Karteris, M (2002) Agreement assessment of NOAA/AVHRR NDVI with Landsat TM NDVI for mapping burned forested areas. *International Journal of Remote Sensing* **23**, 4235-4246.

Escuin, S, Navarro, R, Fernández, P (2007) Fire severity assessment by using NBR (Normalized Burn Ratio) and NDVI (Normalized Difference Vegetation Index) derived from LANDSAT TM/ETM images. *International Journal of Remote Sensing* **29**, 1053-1073.

Fraser, RH, Li, Z, Cihlar, J (2000) Hotspot and NDVI Differencing Synergy (HANDS): A New Technique for Burned Area Mapping over Boreal Forest. *Remote sensing of environment* **74**, 362-376.

Giglio, L, Descloitres, J, Justice, CO, Kaufman, YJ (2003) An enhanced contextual fire detection algorithm for MODIS. *Remote sensing of environment* **87**, 273-282.

Giglio, L, Randerson, J, Van der Werf, G, Kasibhatla, P, Collatz, G, Morton, D, DeFries, R (2010) Assessing variability and long-term trends in burned area by merging multiple satellite fire products. *Biogeosciences* **7**.

Giglio, L, Van der Werf, G, Randerson, J, Collatz, G, Kasibhatla, P (2006) Global estimation of burned area using MODIS active fire observations. *Atmospheric Chemistry and Physics* **6**, 957-974.

Hawbaker, TJ, Radeloff, VC, Syphard, AD, Zhu, Z, Stewart, SI (2008) Detection rates of the MODIS active fire product in the United States. *Remote sensing of environment* **112**, 2656-2664.

Huang, X, Li, M, Li, J, Song, Y (2012) A high-resolution emission inventory of crop burning in fields in China based on MODIS Thermal Anomalies/Fire products. *Atmospheric Environment* **50**, 9-15.

Justice, C, Giglio, L, Korontzi, S, Owens, J, Morisette, J, Roy, D, Descloitres, J, Alleaume, S, Petitcolin, F, Kaufman, Y (2002) The MODIS fire products. *Remote sensing of environment* **83**, 244-262.

Kasischke, ES, Hewson, JH, Stocks, B, van der Werf, G, Randerson, J (2003) The use of ATSR active fire counts for estimating relative patterns of biomass burning–a study from the boreal forest region. *Geophysical Research Letters* **30**.

Kaufman, YJ, Justice, CO, Flynn, LP, Kendall, JD, Prins, EM, Giglio, L, Ward, DE, Menzel, WP, Setzer, AW (1998) Potential global fire monitoring from EOS-MODIS. *Journal of Geophysical Research: Atmospheres (1984–2012)* **103**, 32215-32238.

Key, C, Benson, N (1999) 'Measuring and remote sensing of burn severity, Proceedings joint fire science conference and workshop.'

Lin, H-W, Jin, Y, Giglio, L, Foley, JA, Randerson, JT (2012) Evaluating greenhouse gas emissions inventories for agricultural burning using satellite observations of active fires. *Ecological Applications* **22**, 1345-1364.

McCarty, J, Justice, C, Korontzi, S (2007) Agricultural burning in the Southeastern United States detected by MODIS. *Remote sensing of environment* **108**, 151-162.

McCarty, JL (2011) Remote sensing-based estimates of annual and seasonal emissions from crop residue burning in the contiguous United States. *Journal of the Air & Waste Management Association* **61**, 22-34.

Randerson, JT, Chen, Y, van der Werf, GR, Rogers, BM, Morton, DC (2012) Global burned area and biomass burning emissions from small fires. *Journal of Geophysical Research: Biogeosciences* **117**, G04012.

Romanenkov, V, Rukhovich, D, Koroleva, P, McCarty, JL (2014) Estimating Black Carbon Emissions from Agricultural Burning. In 'Novel Measurement and Assessment Tools for Monitoring and Management of Land and Water Resources in Agricultural Landscapes of Central Asia.' pp. 347-364.

Rouse Jr, JW, Haas, R, Schell, J, Deering, D (1974) Monitoring vegetation systems in the Great Plains with ERTS. *NASA special publication* **351**, 309.

Roy, D, Boschetti, L, Justice, C, Ju, J (2008) The collection 5 MODIS burned area product—Global evaluation by comparison with the MODIS active fire product. *Remote sensing of environment* **112**, 3690-3707.

Roy, D, Landmann, T (2005) Characterizing the surface heterogeneity of fire effects using multi-temporal reflective wavelength data. *International Journal of Remote Sensing* **26**, 4197-4218.

Roy, D, Lewis, P, Justice, C (2002) Burned area mapping using multi-temporal moderate spatial resolution data—A bi-directional reflectance model-based expectation approach. *Remote sensing of environment* **83**, 263-286.

Roy, DP, Boschetti, L (2009) Southern Africa validation of the MODIS, L3JRC, and GlobCarbon burned-area products. *Geoscience and Remote Sensing, IEEE Transactions on* **47**, 1032-1044.

Sharma, AR, Kharol, SK, Badarinath, K (2009) Satellite observations of unusual dust event over North-East India and its relation with meteorological conditions. *Journal of Atmospheric and Solar-Terrestrial Physics* **71**, 2032-2039.

Smith, AM, Wooster, MJ, Drake, NA, Dipotso, FM, Falkowski, MJ, Hudak, AT (2005) Testing the potential of multi-spectral remote sensing for retrospectively estimating fire severity in African Savannahs. *Remote sensing of environment* **97**, 92-115.

Stronach, NR, McNaughton, S (1989) Grassland fire dynamics in the Serengeti ecosystem, and a potential method of retrospectively estimating fire energy. *Journal of Applied Ecology* 1025-1033.

Stroppiana, D., Bordogna, G., Boschetti, M., Carrara, P., Boschetti, L., & Brivio, P. A. (2012). Positive and negative information for assessing and revising scores of burn evidence. *Geoscience and Remote Sensing Letters* **9**, 363-367.

Trigg, S, Flasse, S (2001) An evaluation of different bi-spectral spaces for discriminating burned shrub-savannah. *International Journal of Remote Sensing* **22**, 2641-2647.

Watts, JD, Lawrence, RL, Miller, PR, Montagne, C (2009) Monitoring of cropland practices for carbon sequestration purposes in north central Montana by Landsat remote sensing. *Remote sensing of environment* **113**, 1843-1852.

Williams, KR (1991) Hills of gold: a history of wheat production technologies in the Palouse region of Washington and Idaho. Washington State University.

Woodcock, CE, Allen, R, Anderson, M, Belward, A, Bindschadler, R, Cohen, W, Gao, F, Goward, SN, Helder, D, Helmer, E (2008) Free access to Landsat imagery. *Science (New York, NY)* **320**, 1011.

Zhang, X, Kondragunta, S (2008) Temporal and spatial variability in biomass burned areas across the USA derived from the GOES fire product. *Remote sensing of environment* **112**, 2886-2897.

Appendix: Description of Data and Processing

This appendix describes the VALERI protocol (Baret *et al.* 2005) used to collect ground measurements in detail as well as providing a greater description of collected data sets used in the chapter 2 analyses.

VALERI protocol

The protocol established by Baret *et al.* (2005) is presented as a basis for validating medium resolution satellite products. In their document, the authors outline necessary measurements to be considered based on a site's size, homogeneity, topography and biome type. The spatial sampling schemes for an established site, which they refer to as elementary sampling unit (ESU) also depends on the before mentioned parameters. Since Landsat 8 OLI exists at a higher spatial resolution than the medium resolution sensors they address, we followed methodology for scaling high spatial resolution imagery. This means we scaled only once as opposed to multiple scaling up or down multiple levels.

For our analysis, ESUs were established in the field based on scaling parameters necessary for Landsat 8 OLI and to account for factors which could bias results (e.g. local topography and man-made elements). These sites were established in mid-June after the growing season had already begun. The spatial sampling contained within one ESU is presented (Fig.7). We adapted the spatial sampling scheme by combining the "square" and "cross" patterns for our sites. As our crop sites were neither sparse nor discontinuous in vegetation distribution, this method was deemed optimal for our needs.

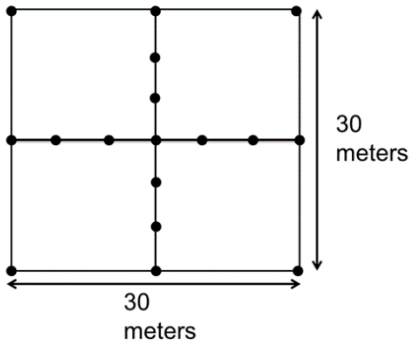

Fig. 7. Established ESU for sampling protocol. One ESU is established for the Landsat 8 OLI pixel of interest. Center pixel coordinates are taken from the center individual sampling site where the crossed transects intersect.

Data processing

The steps taken for ground data processing are presented in a conceptual diagram (Fig. 8). The relative spectral response functions used to average the ASD data into Landsat 8 OLI surface reflectance values were downloaded from NASA Landsat website: (http://landsat.gsfc.nasa.gov/?p=5779).

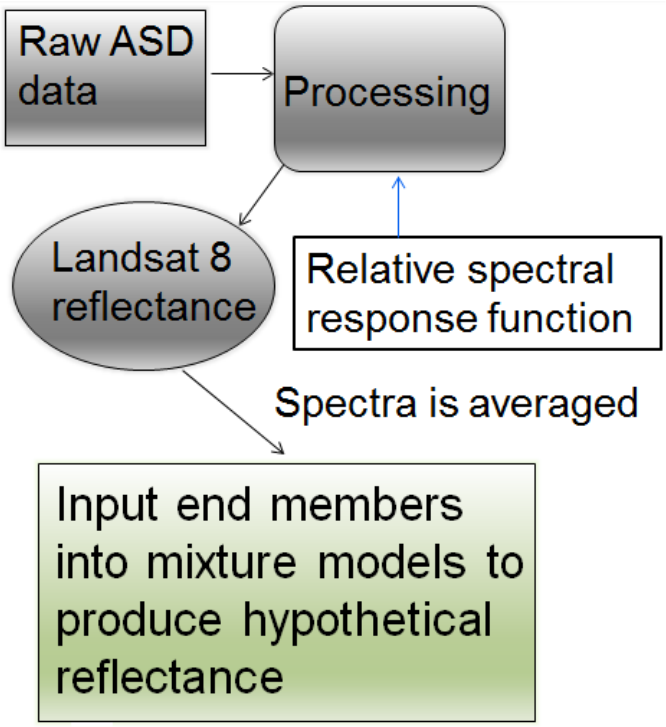

Fig.8. Conceptual diagram of processing procedure from binary ASD data to usable endmember inputs.

Coincident Landsat 8 overpass data is represented (Table 7). Ground measurements were taken throughout the summer at each of the overpass dates with interest in characterizing the similarity of ground obtained ASD measurements with Landsat 8 OLI overpass data.

Table 7. Coincident Landsat 8 OLI scene with date of overpass and ground collection.

Landsat 8 OLI scene	Date of overpass / ground collection	Sites sampled
LC80430272014182LGN00	July 1	A,B,C,D
LC80420282014191LGN00	July 10	A,B,C,D
LC80430272014198LGN00	July 17	A,B,C,D
LC80420282014207LGN00	July 26	A,B,C,D
LC80430272014214LGN00	August 2	A,B,C,D
LC80420282014223LGN00	August 11	A,B,C,D
LC80430272014230LGN00	August 18	A,B,C,D
LC80420282014239LGN00	August 27	A,B,C,D
LC80420282014255LGN00	September 12	E,F

The results of each scatter plot r^2 value are presented in Table 8. The comparison revealed the weakest correlation existing in the NIR channel. We expect that this correlation may have been influenced by site disturbances to sampling throughout the summer.

Table 8. R-squared values for comparison of Landsat 8 OLI overpass data and ASD averaged data. Bands in bold are channels used in analyisis.

Landsat 8 OLI band	R-Squared value
Band 2	0.834
Band 3	0.908
Band 4	0.9414
Band 5	0.6818
Band 6	0.9221
Band 7	0.8963

Site B which had the experienced the heaviest disturbance, had a number of flattened areas throughout the pixel surface caused by nesting wildlife (Fig.9). We suspect that this disturbance is the reason for the least comparability among all the sites (r^2=0.06).

Fig 9. Hemispherical image taken from within site B on July 1st, 2014. The image shows heavy disturbance of vegetation structure which was typical throughout the site. Hemispherical lens was used as subsequent sampling of LAI was taking place for other studies.